Electronic Supplementary Material (ESI) for Journal of Materials Chemistry C.

Supplemental Information for

Opto-electronic coupling in semiconductors: towards ultra-sensitive pressure sensing

Thanh Nguyen,[a] Toan Dinh,[a] Hoang-Phuong Phan,[a] Tuan-Khoa Nguyen,[a] Abu Riduan Md Foisal,[a] Nam-Trung Nguyen,[a] and Dzung Viet Dao[ab*]

[a] *Queensland Micro and Nanotechnology Centre, Griffith University, Queensland, Australia, E-mail: d.dao@griffith.edu.au*
[b] *School of Engineering and Built Environment, Griffith University, Queensland, Australia.*

1 Comparison of the sensitivity of the pressure sensor in this work and literature.

Table S1: Comparison of the sensitivity of the pressure sensor in this work and literature.

Material	Sensitivity	Pressure range	Principle	Diaphragm geometry	Refs
4H-SiC	10.83×10^{-5} kPa^{-1}	90÷300 kPa	Piezoresistive	Square: 5mm× 5mm×70μm	1
3C-SiC nanowire	5×10^{-4} kPa^{-1}	10÷50 kPa	Piezoresistive	Square: 5mm× 5mm×150μm	2
Si Single crystalline	3.2×10^{-4} kPa^{-1}	-20÷20 kPa	Piezoresistive	Cantilever	3
Si Single crystalline	2.4×10^{-4} kPa^{-1}	0÷100 kPa	Piezoresistive	Radius: 20 μm Thickness: 1.2 μm	4
Si polysilicon nanofilm	2.896×10^{-5} kPa^{-1}	$<$ 2.5 MPa	Piezoresistive	Rectangular: 0.3mm× 1.5mm×6.3μm	5
n-type 4H-SiC	2.68×10^{-6} kPa^{-1}	$<$ 6000 kPa	Piezoresistive	Radius: 1 mm Thickness: 50 μm	6
3C-SiC/Si	0.87 kPa^{-1}	5÷70 kPa	Opto-electronic coupling	Square: 5mm× 5mm×225μm	This work

Although the diaphragm in this work was quite thick compared to previous reports (such as 225μm compared with 150 μm and 70 μm[1,2]), the sensitivity of the sensor was much higher than that of previous ones. The ensitivity of the pressure sensor in this work is more than 1,700 times higher than the best results shown in the above table[2].

2 Pressure sensor design

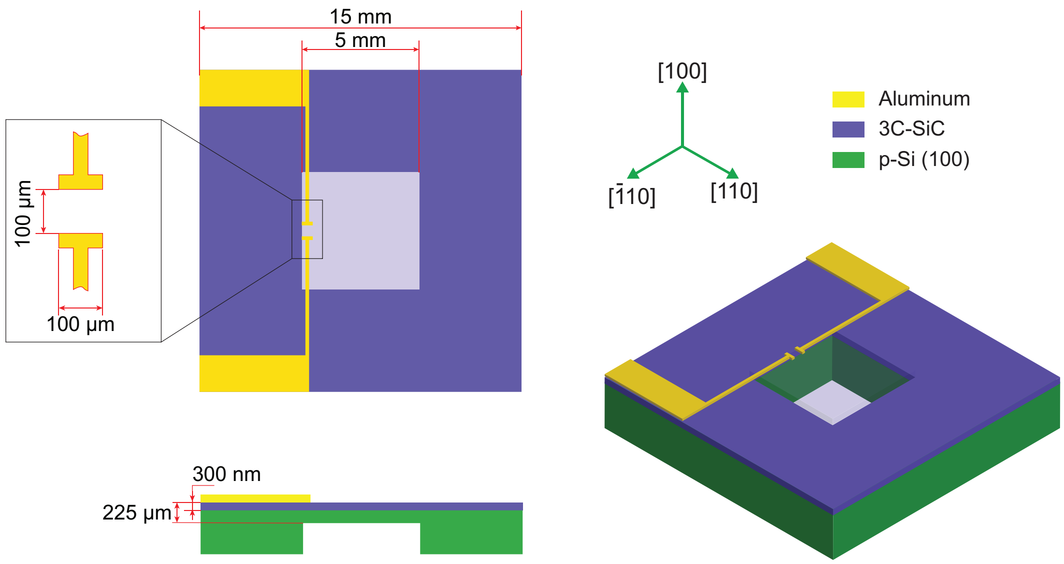

Figure S1: Pressure sensor design.

Geometry of the diaphragm: Circular diaphragm and rectangular diaphragm are two common types of diaphragm used in designs of micromachined pressure sensors. With the same chip size, the pressure sensor with a square diaphragm has maximum stress/strain of 1.64 times higher, hence 1.64 times more sensitive, compared to a circle one. Moreover, a square diaphragm is more suitable for anisotropic wet etching method. Thus, in this research, a square diaphragm was used in our design.

Position and direction of the piezoresistor: In term of location and direction of sensing element, to maximize the sensitivity of the pressure sensor, the sensing element is fabricated at middle of the edge of the diaphragm where induced tress/strain is maximum, and the piezoresistor is aligned or perpendicular with maximum piezoresistive coefficient directions. With using material p-type 3C-SiC/Si (100) whose maximum piezoresistive coefficient direction is [110], the piezoresistor was aligned in [110] direction in our pressure. In this prototype, instead of integrating light source in the pressure sensor, we used external light source which is simple for controlling light beam position and light intensity.

3 Characteristics of the 3C-SiC thin film grown on the Si substrate

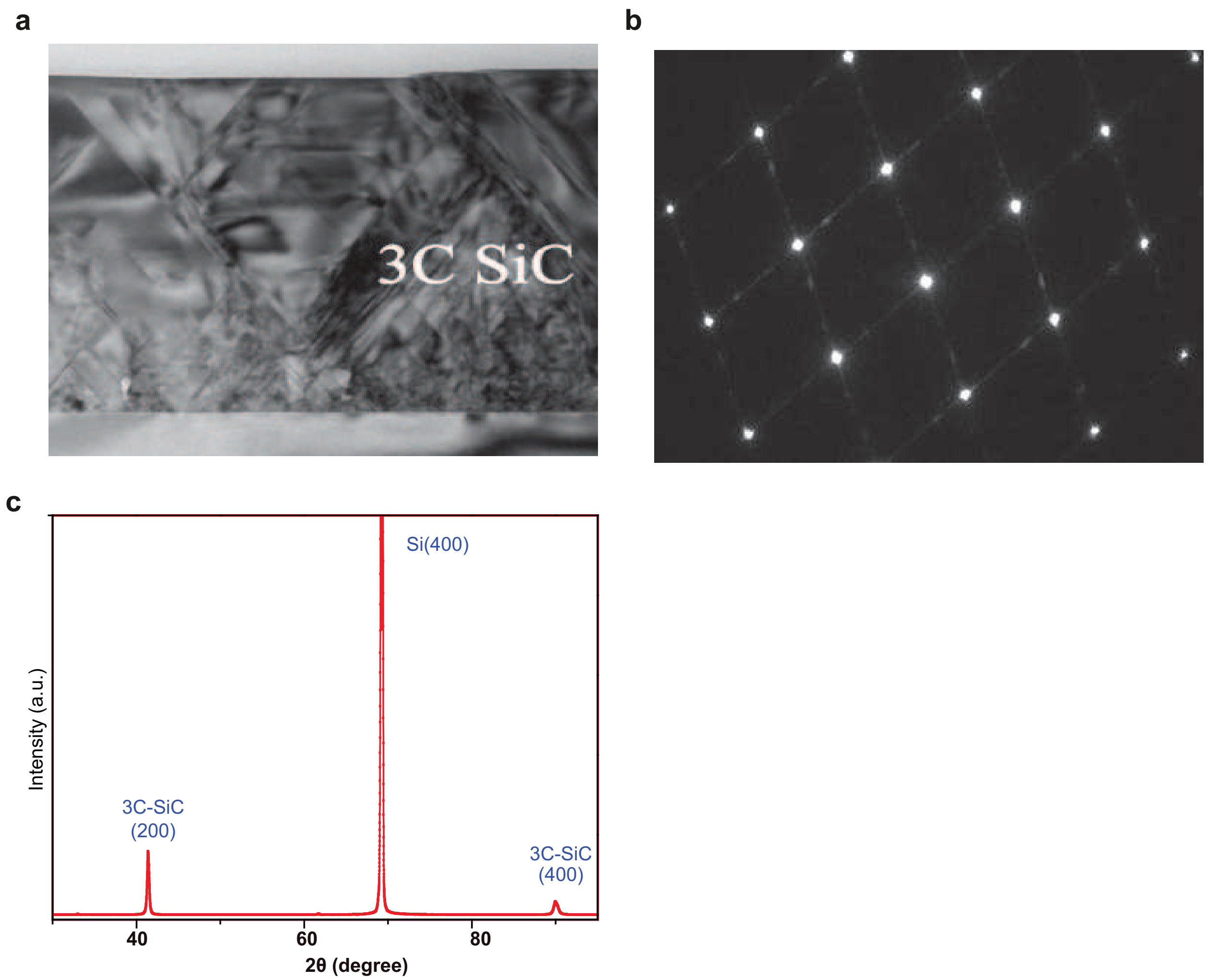

Figure S2: Characteristics of the 3C-SiC thin film grown on the Si substrate. (A) TEM image of 3C-SiC grown on the Si. **(B)** SAED image of the 3C-SiC. **(C)** XRD graph of 3C-SiC grown on the Si.

4 Pressure sensors

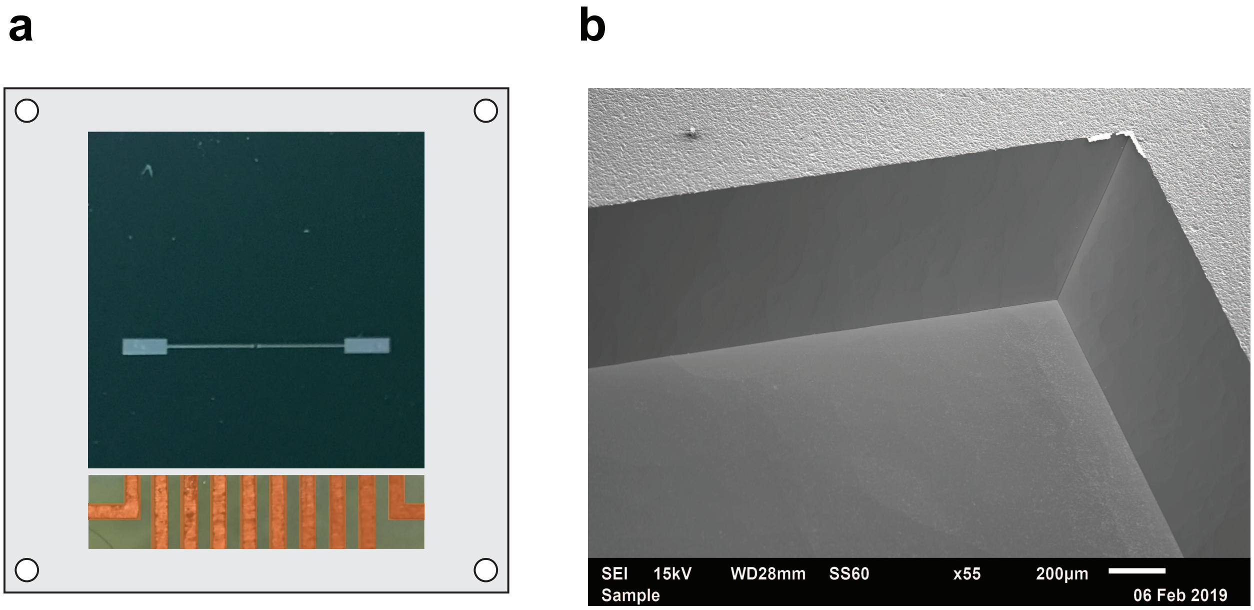

Figure S3: (a) The pressure sensor after attaching to an acrylic holder. **(b)** The Scanning Electron Microscope (SEM) image of the back side of the diaphragm.

5 Performance characterisation

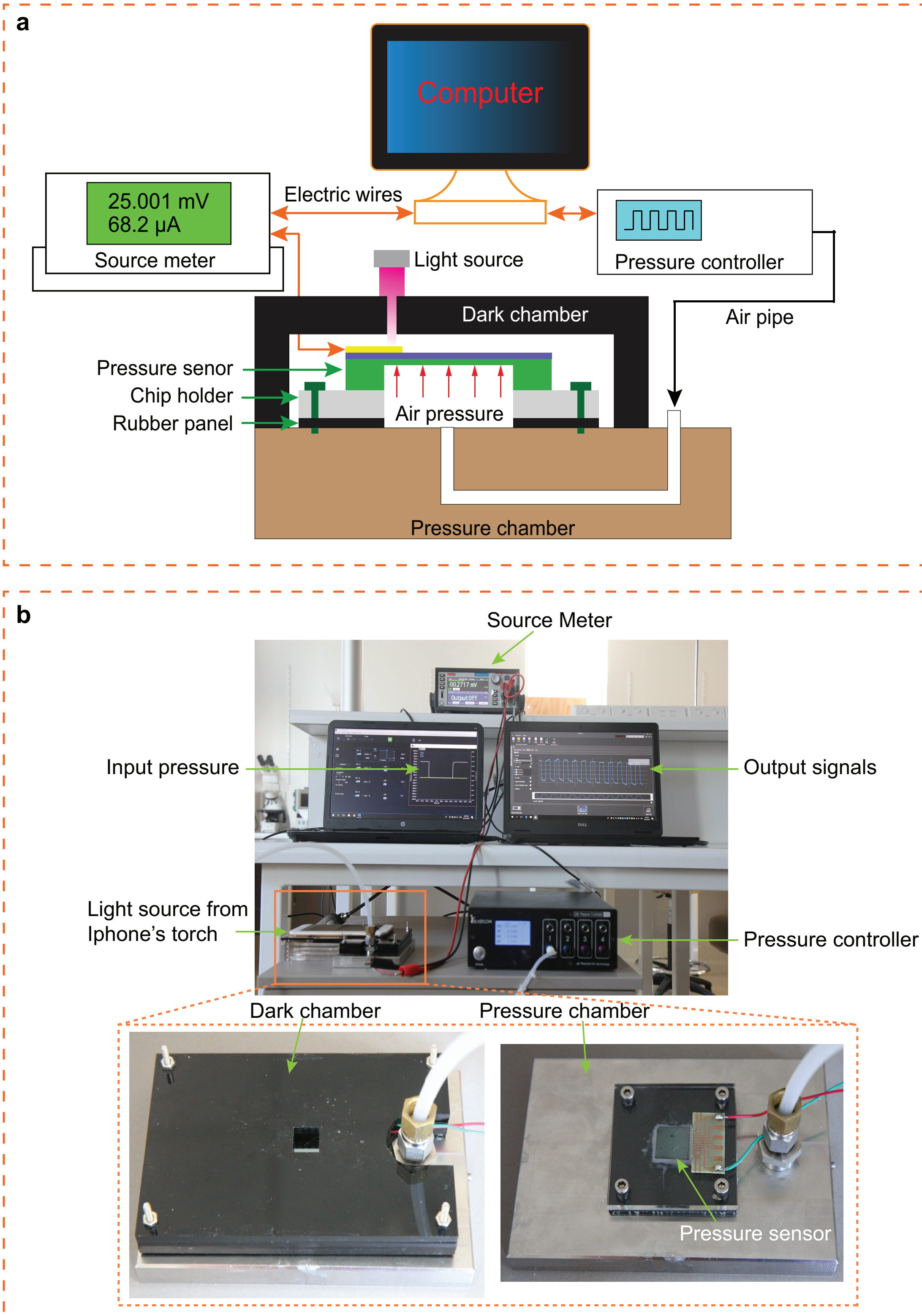

Figure S4: (a) Experimental schematic and (b) Experimental setup. The pressure sensor was mounted on the surface of a pressure chamber. The air pressure was accurately controlled by an ELVEFLOW OB1 pressure controller and applied to the back side of the diaphragm. A dark chamber was used to isolate the pressure sensor from unwanted background light. The visible light illuminated on the surface of the sensing element via a small window on the roof of the chamber. The tuning current was accurately controlled by a Keithley 2450 SourceMeter, which was simultaneously utilized for measuring voltage. Both the source meter and pressure controller were connected to computer for data collection.

6 Photovoltage and photocurrent

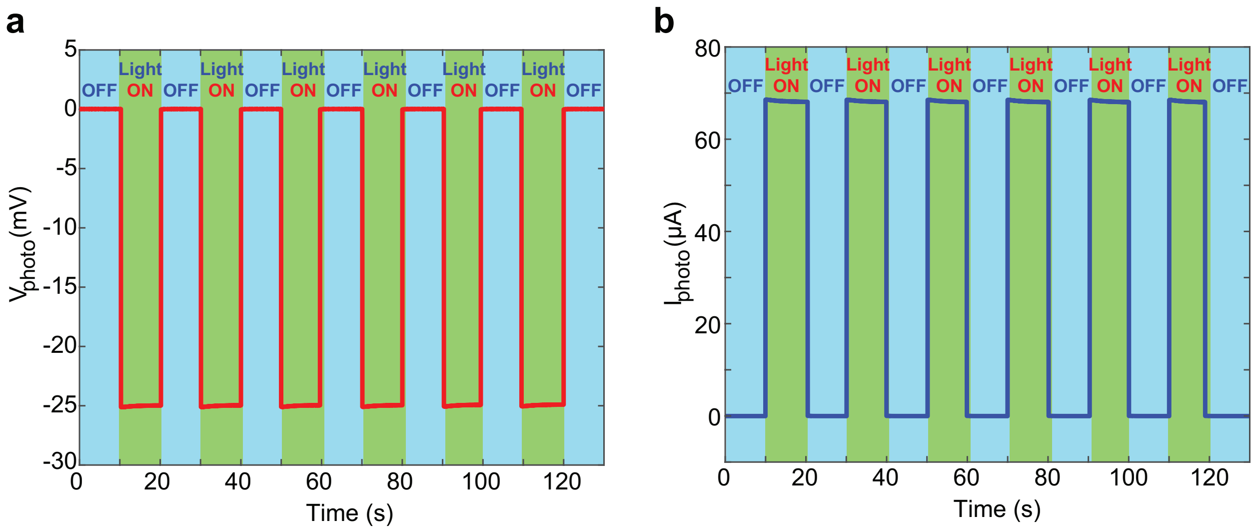

Figure S5: The repeatabilities of photocurrent and lateral photovoltage. The repeatability of the photocurrent and lateral photovoltage in the sensing element when the non-uniform visible light was periodically turned ON and OFF. The excellent repeatability of photocurrent and lateral photovoltage were observed. **(a)** As the light was turned OFF, the photocurrent was 0 μA, while this value was approximately 68.2 μA under the light illumination. **(b)** The lateral photovoltage was 0 mV under darkness, and around -25 mV under the light condition.

7 Tunability of the sensitivity

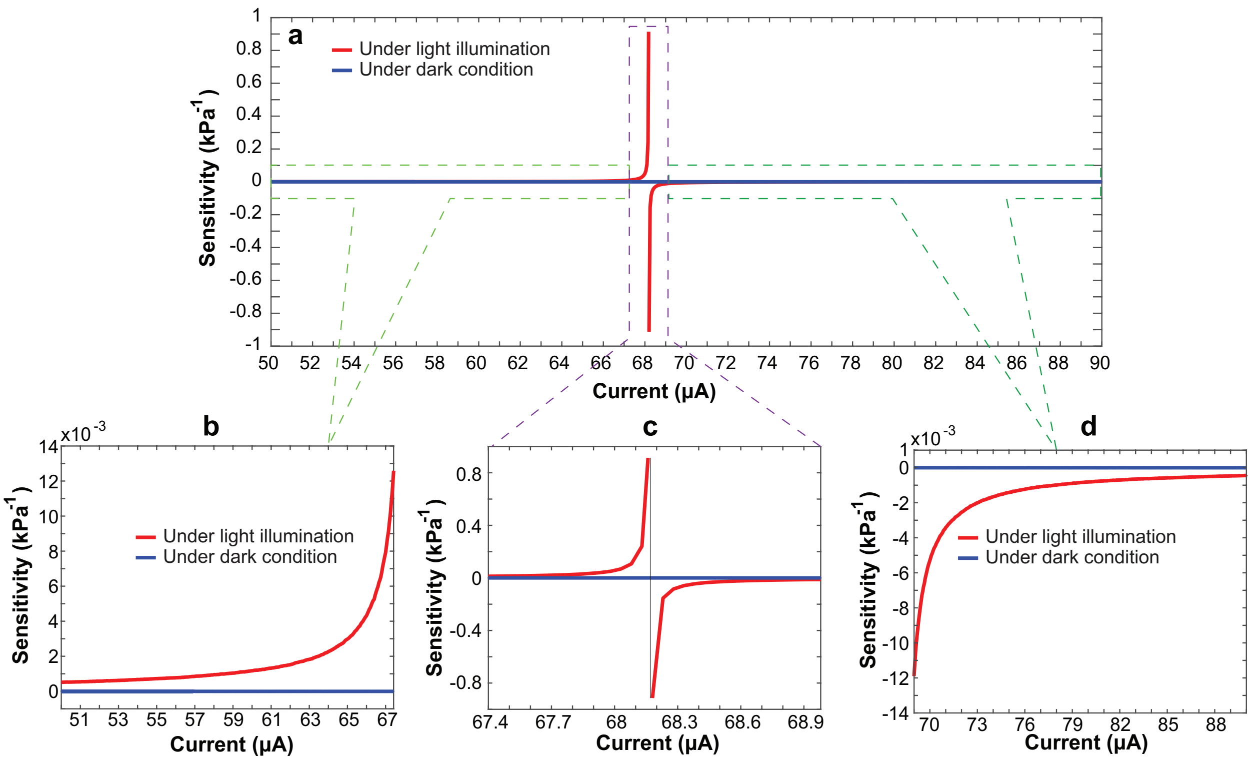

Figure S6: Effect of the tuning current on enhancing pressure sensitivity by opto-electronic coupling. **(a)** The pressure sensitivity versus the tuning current on whole range of the tuning current. Sensitivity of the pressure sensor significantly changed versus the tuning current under light illumination, while the sensitivity under unilluminated condition is independent of the supplied current. This also demonstrated dependence of piezoresistive effect on the tuning current under the illuminated condition. Enlarged views of the sensitivity with the tuning current ranging: **(b)** from 50 μA to 67.4 μA; **(c)** from 50 μA to 69 μA, and **(d)** from 69 μA to 90 μA. Under the illuminated condition, when the tuning current increased from 50 μA to 67.4 μA, the pressure sensitivity was positive and rose dramatically from 5.1×10^{-4} kPa^{-1} to 1.22×10^{-2} kPa^{-1}. The sensitivity is highest when the tuning current in the optimal range (50 μA to 69 μA). This sensitivity decreased significantly in the negative range to 3.92×10^{-4} kPa^{-1} when the current increased further to 90 μA.

8 Four-point measurement method

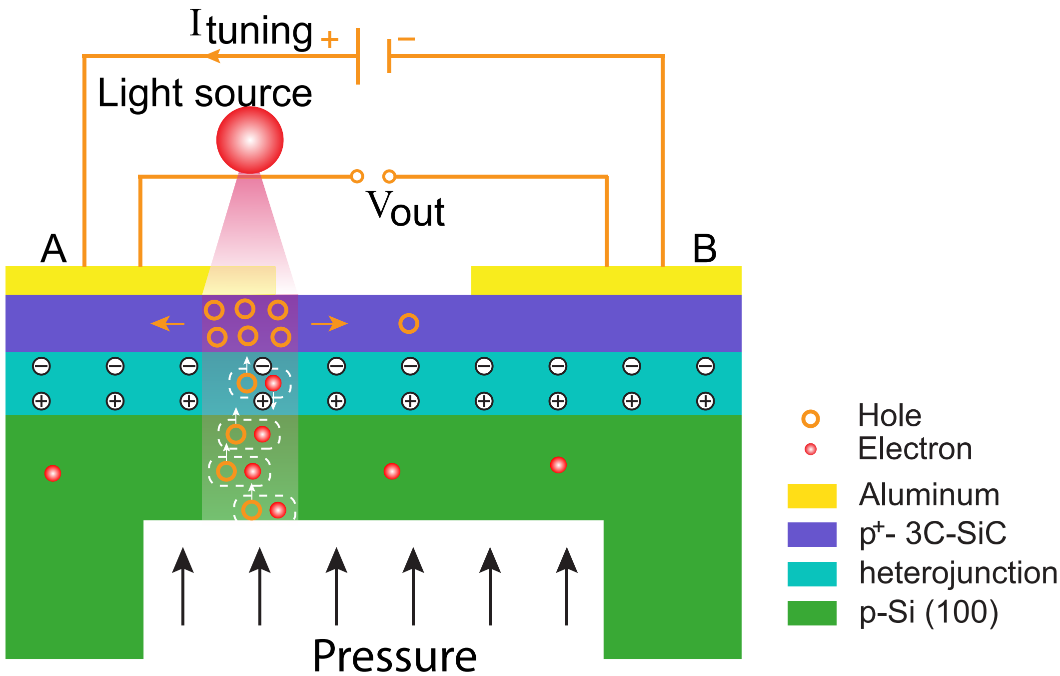

Figure S7: Four-point measurement method.

9 Generation of the photocurrent and redistribution of hole concentration by optimizing the tuning current

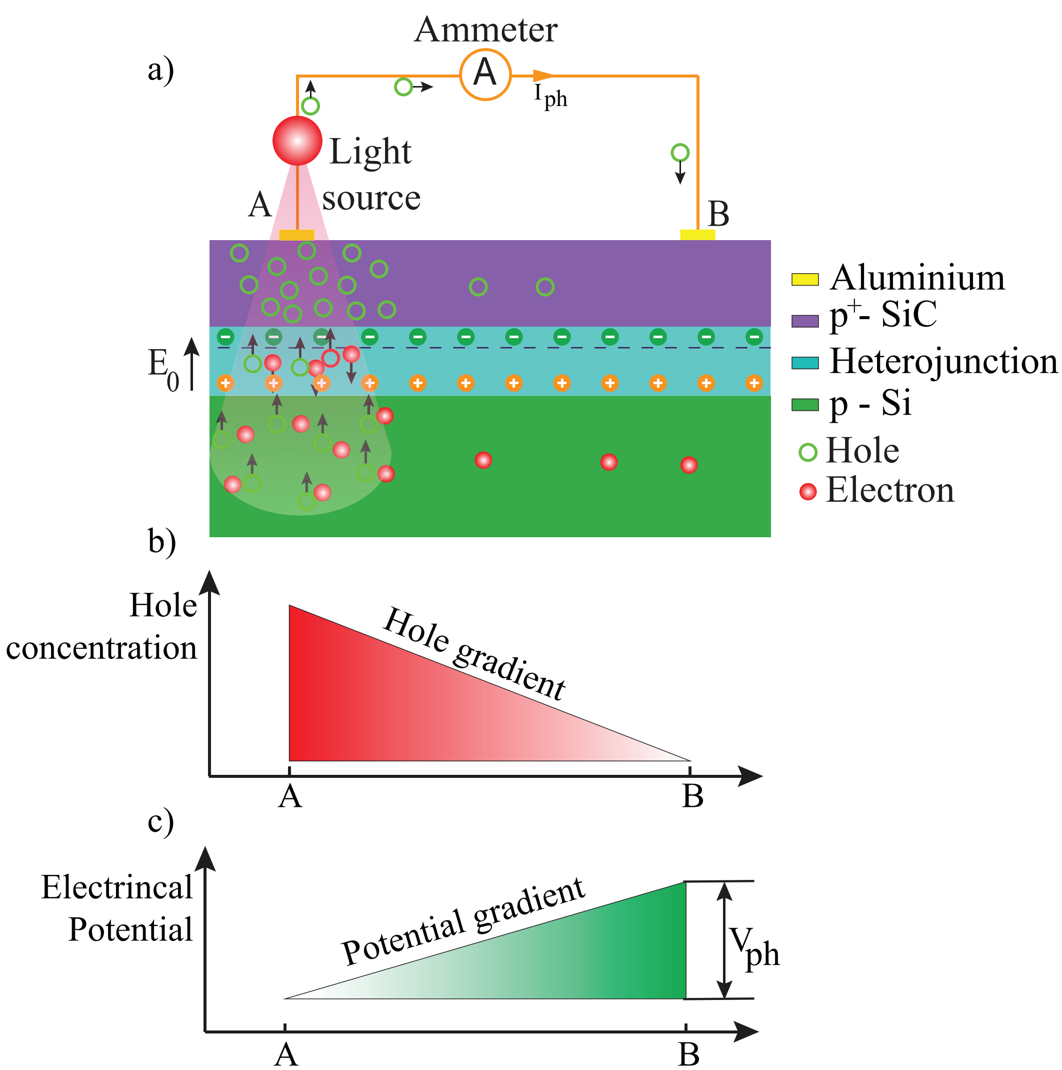

Figure S8: **(a)** The generation of the photocurrent under the illuminated condition. Under the illumination, photons were injected to excite charge carriers (electrons/holes) in the 3C-SiC/Si heterojunction and the Si substrate to generate electron/hole pairs (EHPs). In the heterojunction region, these photogenerated electrons/holes were separated by the built-in electric field E0, where the photogenerated holes and electrons moved toward the 3C-SiC nanofilm and Si substrate, respectively. In addition, photogenerated holes in the Si substrate hypothetically migrated to the 3C-SiC layer by the tunnelling mechanism. As a consequence, the hole concentration in 3C-SiC increased. When the external circuit was shorted, the only current in the circuit was the photocurrent (I_{ph}). **(b)** Hole concentration under nonuniform illumination. The photogenerated holes migrated into 3C-SiC differently in lateral direction, hence resulting in a gradient of hole concentration within the 3C-SiC nanofilm. **(c)** Electrical potential gradient between two electrodes A and B of the sensing element.

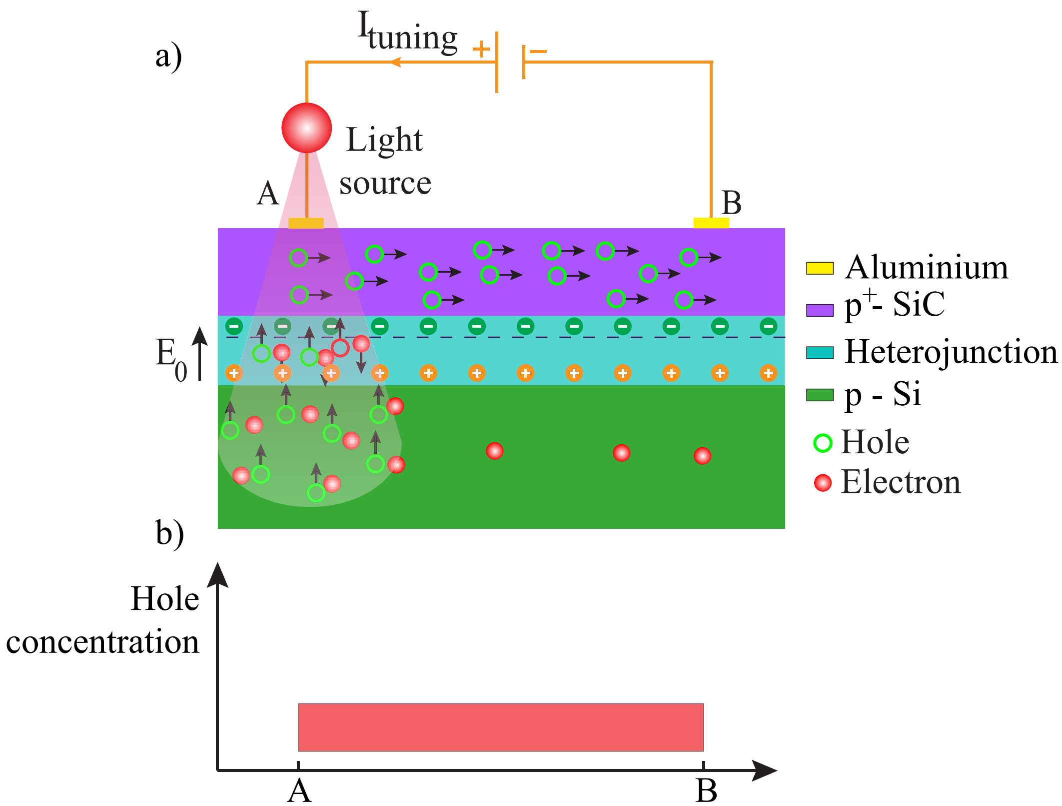

Figure S9: Redistribution of hole carrier by optimizing tuning current. By supplying a tuning current I from electrode A to electrode B of the sensing element, an external electrical field E was created. This external electric field E changed energy of the carriers, hence redistributing the carriers in the 3C-SiC layer. By optimizing the tuning current I, the holes are uniformly redistributed in the 3C-SiC layer from electrode A to electrode B areas, eliminating the gradient of hole concentration. .

10 Long-time stability test results under dark condition

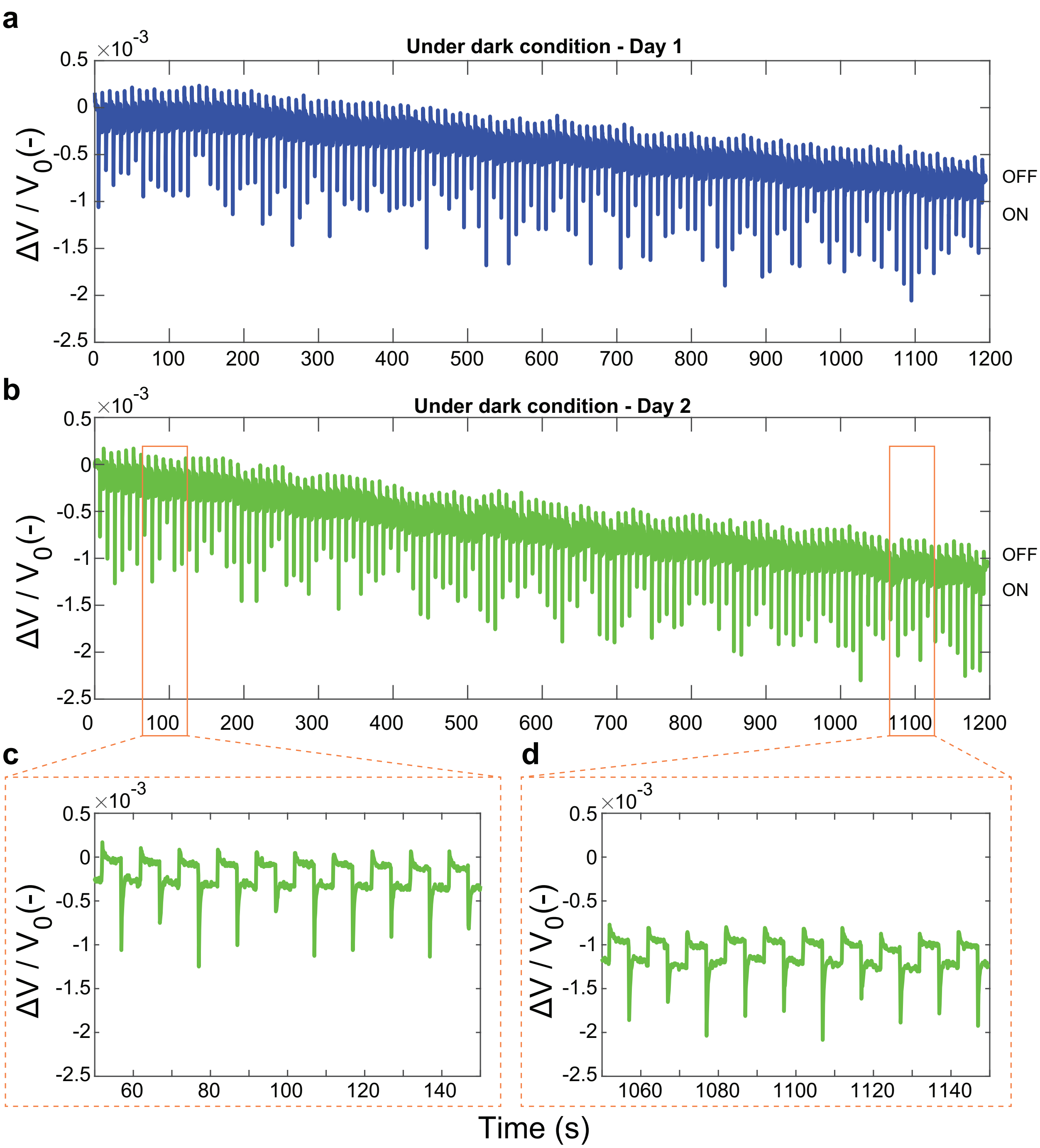

Figure S10: The stability of the pressure sensor under dark condition. The cyclic test was conducted under dark environment in two consecutive days by applying and releasing pressure of 60 kPa. **(a)** and **(b)** are signal responses in the first day and the second day. **(c)** and **(d)** are enlarged views of signal response at the beginning seconds and the ending seconds of the 1000-second recorded result. Although, absolute change of the signal was quite stable over time, the signal drifted significantly over a long duration.

References

1 T.-K. Nguyen, H.-P. Phan, T. Dinh, K. M. Dowling, A. R. M. Foisal, D. G. Senesky, N.-T. Nguyen and D. V. Dao, *Materials & Design*, 2018, **156**, 441–445.

2 H.-P. Phan, K. M. Dowling, T. K. Nguyen, T. Dinh, D. G. Senesky, T. Namazu, D. V. Dao and N.-T. Nguyen, *Materials & Design*, 2018, **156**, 16–21.

3 H. Takahashi, N. M. Dung, K. Matsumoto and I. Shimoyama, *Journal of micromechanics and microengineering*, 2012, **22**, 055015.

4 I. Godovitsyn, V. Amelichev and V. Pankov, *Sensors and Actuators A: Physical*, 2013, **201**, 274–280.

5 J. Wang, R. Chuai, L. Yang and Q. Dai, *Sensors and Actuators A: Physical*, 2015, **228**, 75–81.

6 T. Akiyama, D. Briand and N. F. de Rooij, SENSORS, 2011 IEEE, 2011, pp. 222–225.